

Supporting Information

Superatom-Assembled B₈N₂ Monolayer Acting as an Electronic Sponge for High-Capacity Anode Material of K/Na-Ion Batteries

Kaidong Shen¹, Longjiu Cheng^{1,2,*}, Chang Xu^{1,*}

^a*Department of Chemistry, Anhui University, Hefei, Anhui, 230601, China*

^b*Institutes of Physical Science and Information Technology, Anhui University, Hefei, Anhui, 230601, China*

Contents:

1. **Fig. S1** Graph of K-point test. (Page 2)
2. **Fig. S2-S4** Supplementary diagrams for the B₈N₂ monolayer stability verification. (Page 3-5)
3. **Fig. S6-S8** Supplementary diagrams for verification of the electronic properties of the B₈N₂ monolayer. (Page 5-7)
4. **Fig. S9-S15** Supplementary diagrams of the nature of the B₈N₂ monolayer in alkali metal battery anode material applications. (Page 8-11)
5. **Details** for calculation of free energy difference (ΔG) of the ion migration processes. (Page 12)
6. **Table. S1** Data on the change in bond length and bond angle before and after electron gain and loss for X₄H₄ (X=B₄, C, Si, Ge). (Page 13)
7. **Table S2** The adsorption energies for Li/Na/K ions on the B₈N₂ monolayer calculated with and without van der Waals (VDW) correction. (Page 13)

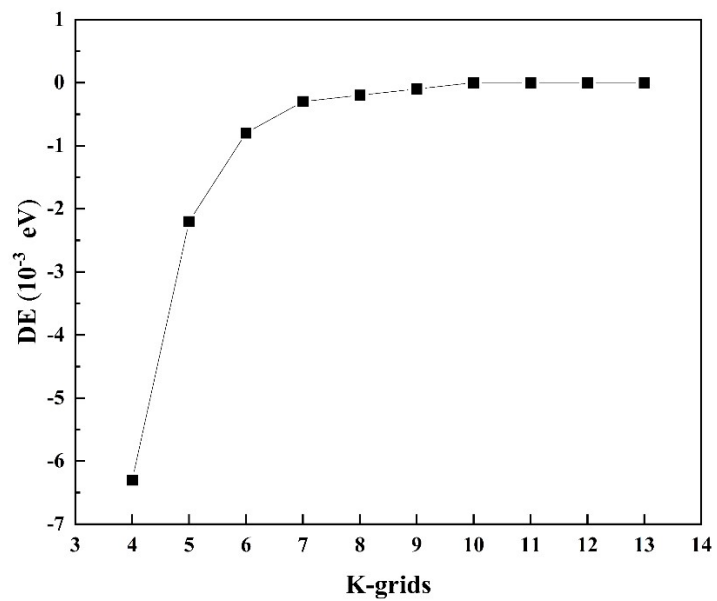


Fig. S1 Differential energy (DE) of a B_4N monolayer as a function of the $n \times n \times 1$ k-point grid.

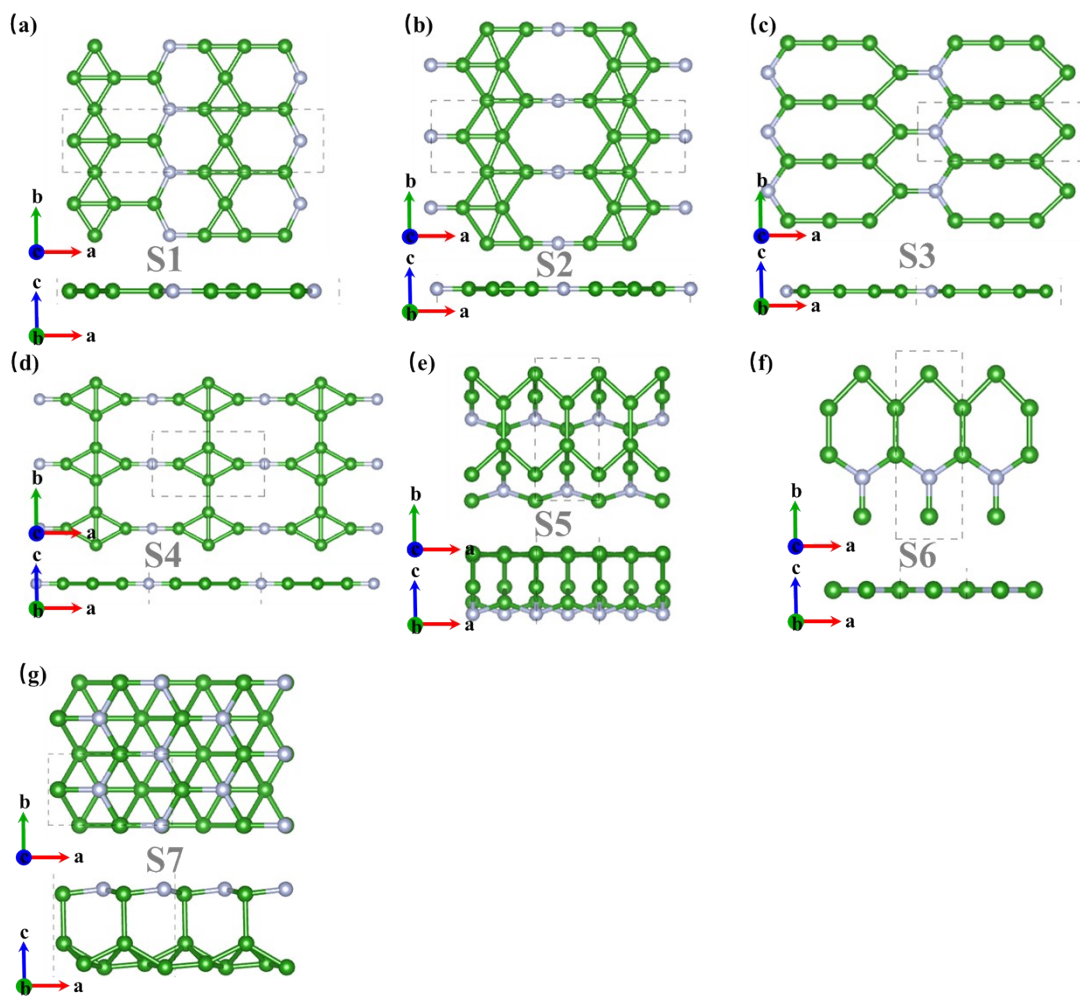


Fig. S2 Stabilized structures searched by the Calypso package based on the B:N=4:1 chemical ratio.

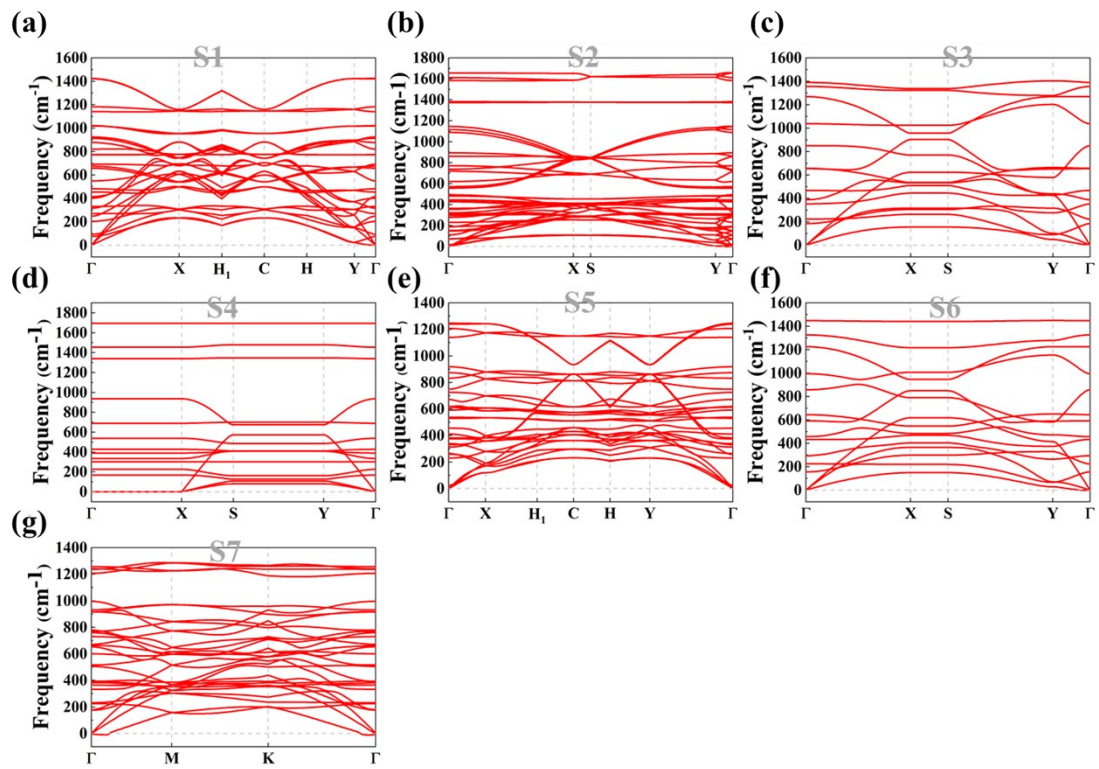


Fig. S3 Phonon spectra of stabilized structures searched by the Calypso software package based on the B:N=4:1 chemical ratio.

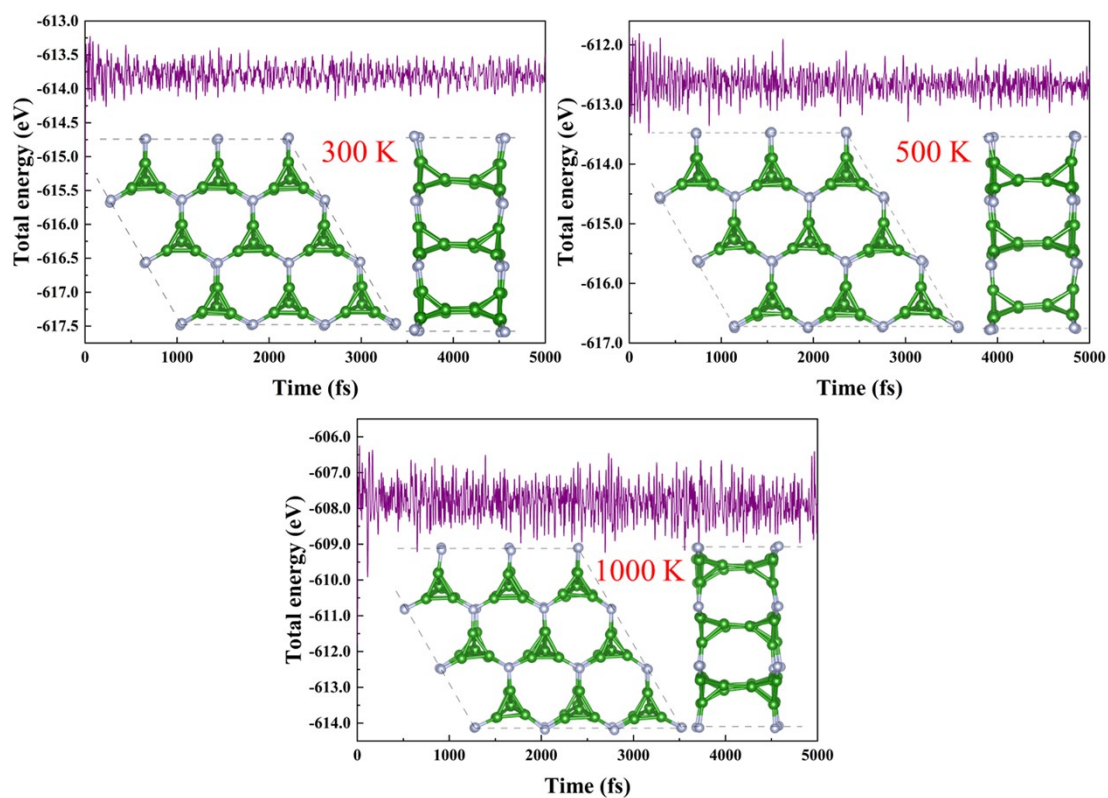


Fig. S4 Total energy for AIMD simulations at 300 K, 500 K and 1000 K. The inset shows the snapshots of the B₄N monolayer taken at the end of the simulation.

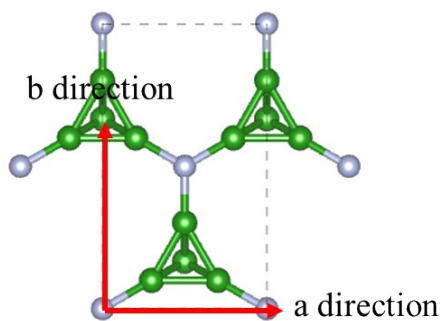


Fig. S5 Orthorhombic cell structure of B₄N monolayers.

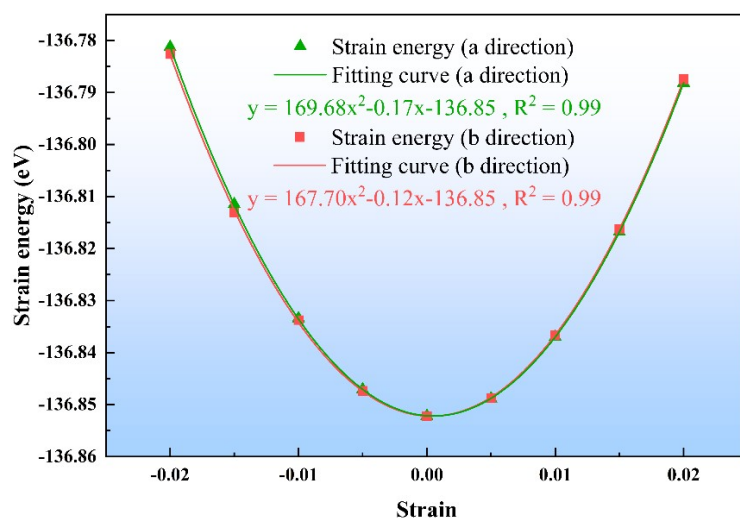


Fig. S6 The polynomial fitting total energy for elastic constant of B₄N monolayer.

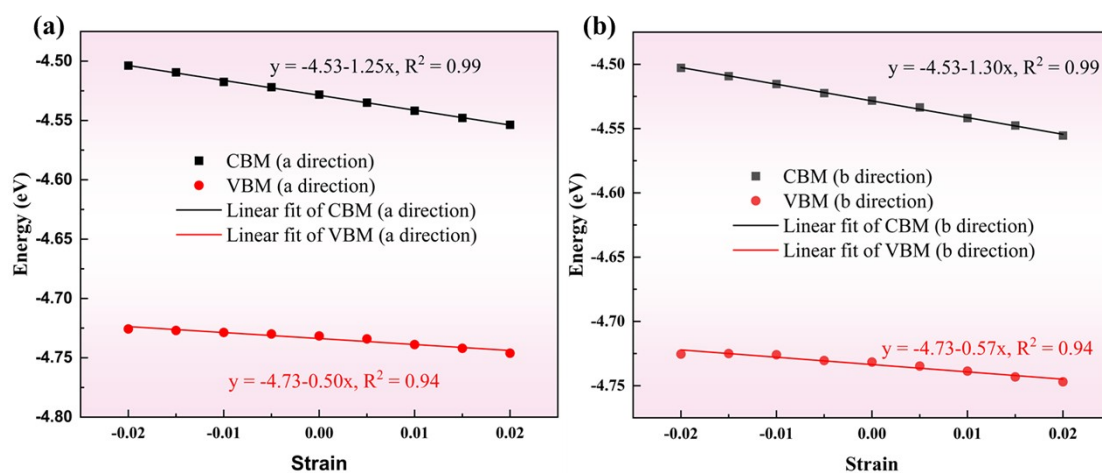


Fig. S7 The linear fitting of VBM and CBM locations of B₄N monolayer corresponding to the applied strain along a and b direction, respectively.

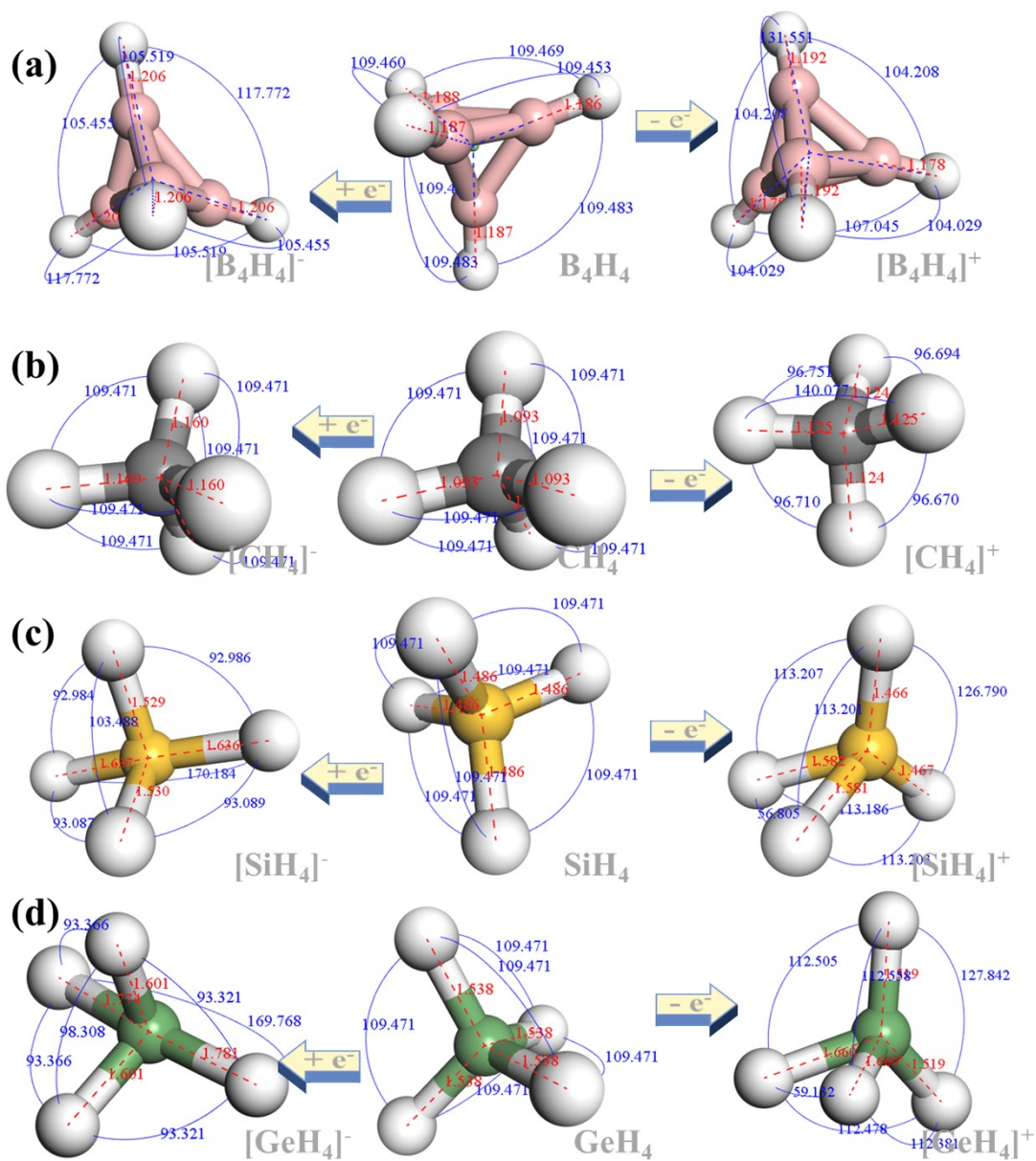


Fig. S8 Optimized structures of XH_4 , $[\text{XH}_4]^-$ and $[\text{XH}_4]^+$ ($\text{X}=\text{B}_4, \text{C}, \text{Si}, \text{Ge}$). The red labeling and blue labeling indicate the key length (in Å) and the key angle (in °), respectively.

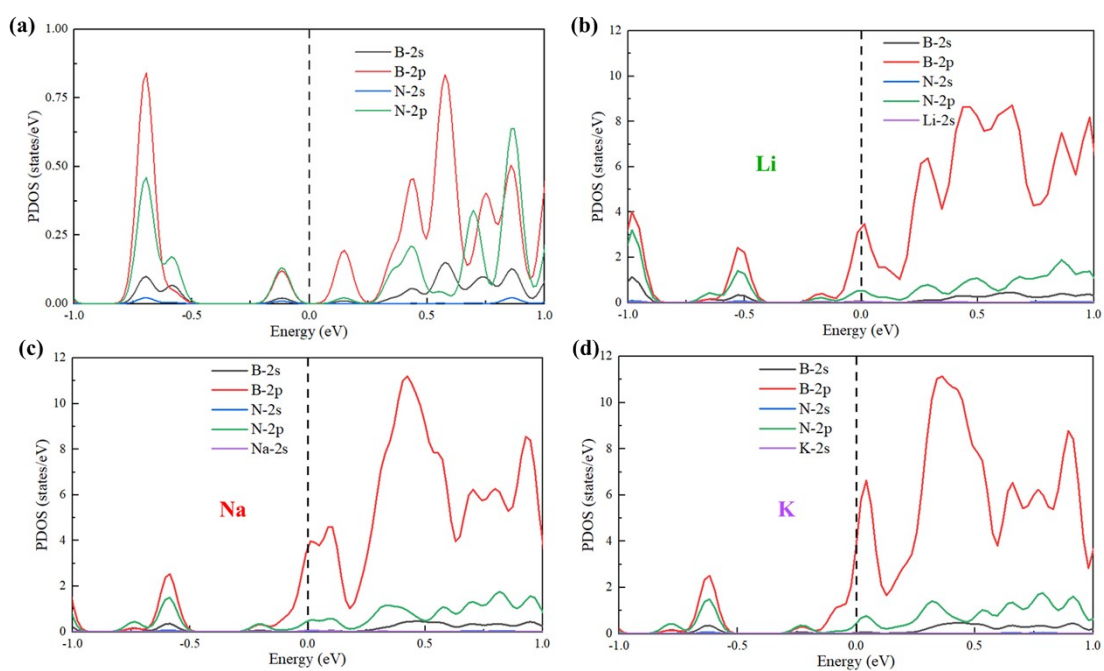


Fig. S9 The calculated PDOS plot of (a) pristine B_4N , (b) $1Li-B_4N$, (c) $1Na-B_4N$ and (d) $1K-B_4N$ at the PBE level. The orange dotted lines denote the locations of the Fermi level.

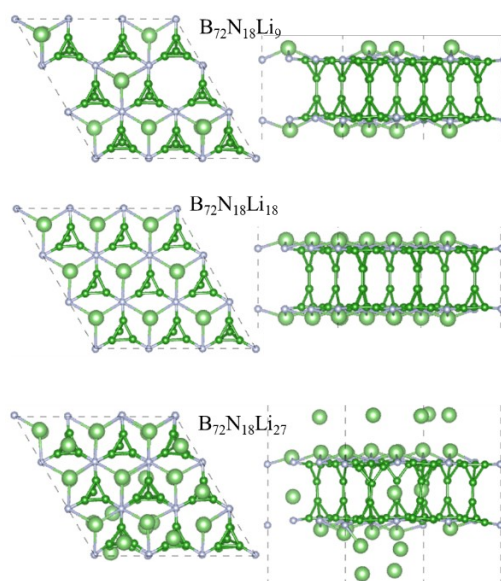


Fig. S10 Top and side views of the geometry of $B_{72}N_{18}Li_9$, $B_{72}N_{18}Li_{18}$ and $B_{72}N_{18}Li_{27}$.

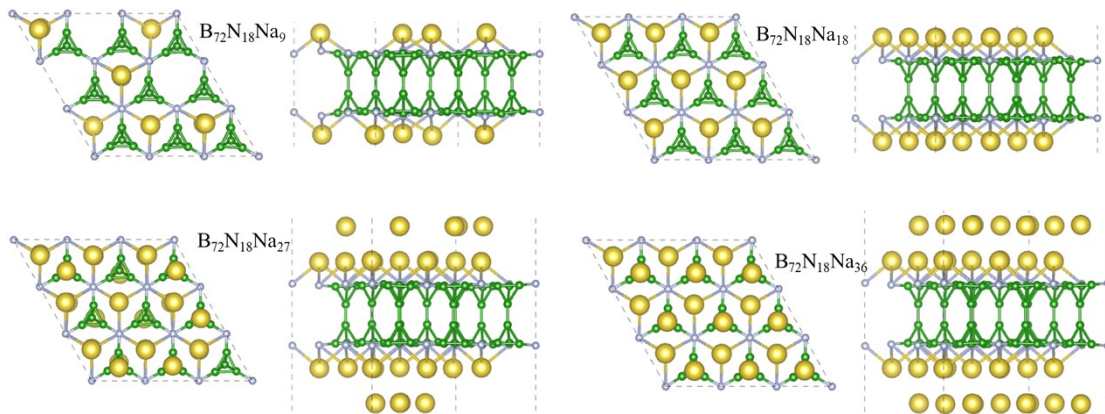


Fig. S11 Top and side views of the geometry of $B_{72}N_{18}Na_9$, $B_{72}N_{18}Na_{18}$, $B_{72}N_{18}Na_{27}$, and $B_{72}N_{18}Na_{36}$.

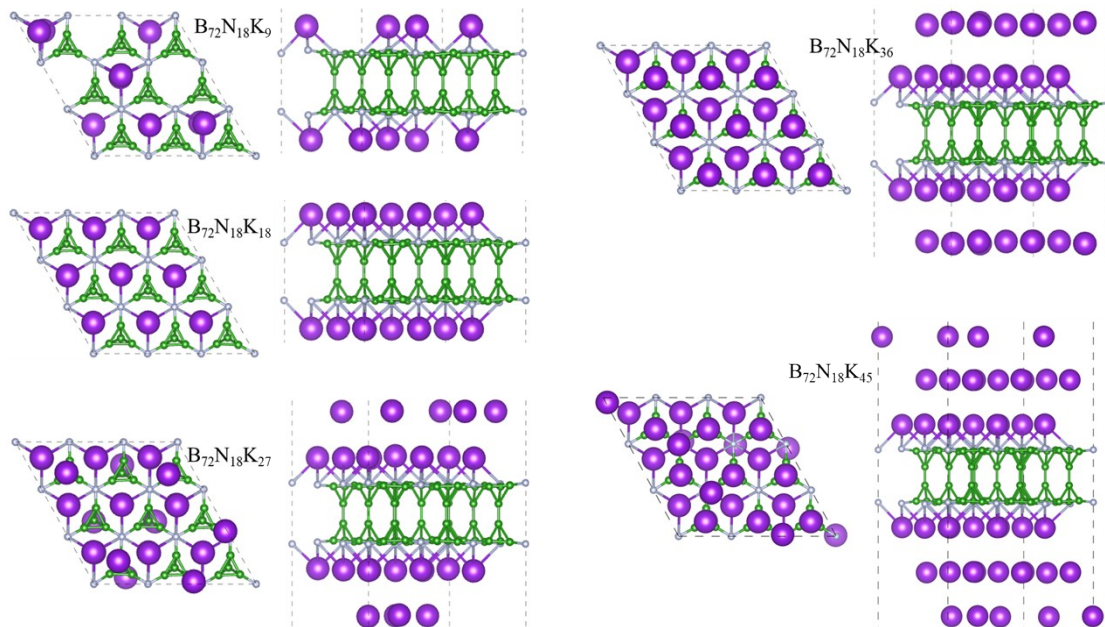


Fig. S12 Top and side views of the geometry of $B_{72}N_{18}K_9$, $B_{72}N_{18}K_{18}$, $B_{72}N_{18}K_{27}$, $B_{72}N_{18}K_{36}$ and $B_{72}N_{18}K_{45}$.

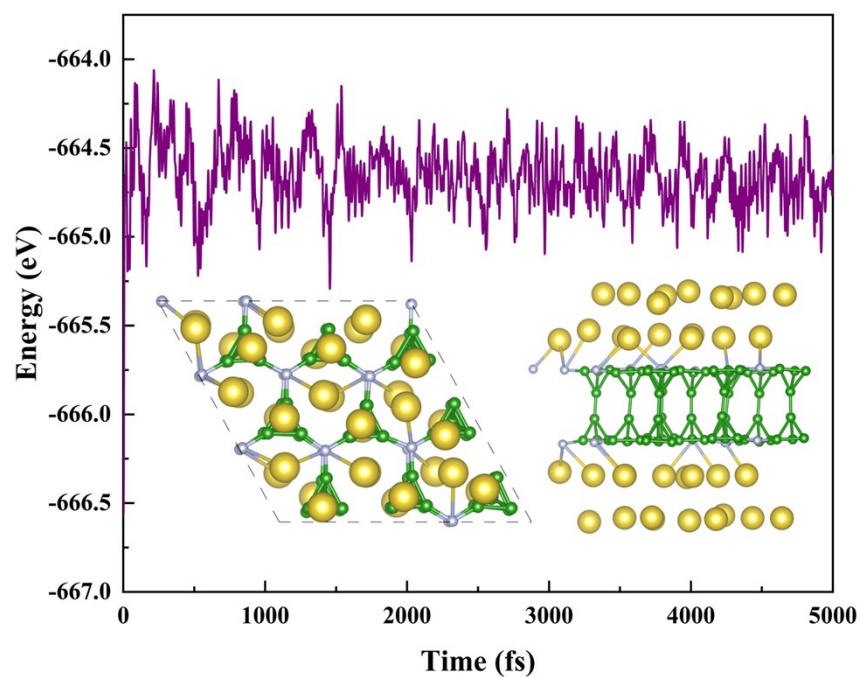


Fig. S13 Total energy during AIMD simulations at 300 K. The inset shows the snapshots of the $B_{72}N_{18}Na_{36}$ monolayer taken at the end of the simulation.

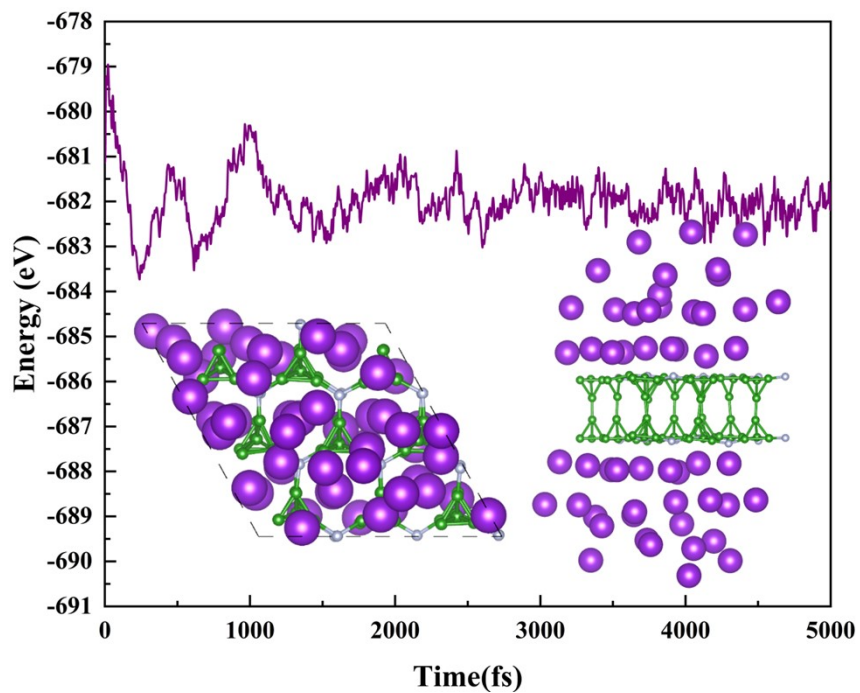


Fig. S14 Total energy during AIMD simulations at 300 K. The inset shows the snapshots of the $B_{72}N_{18}K_{45}$ monolayer taken at the end of the simulation.

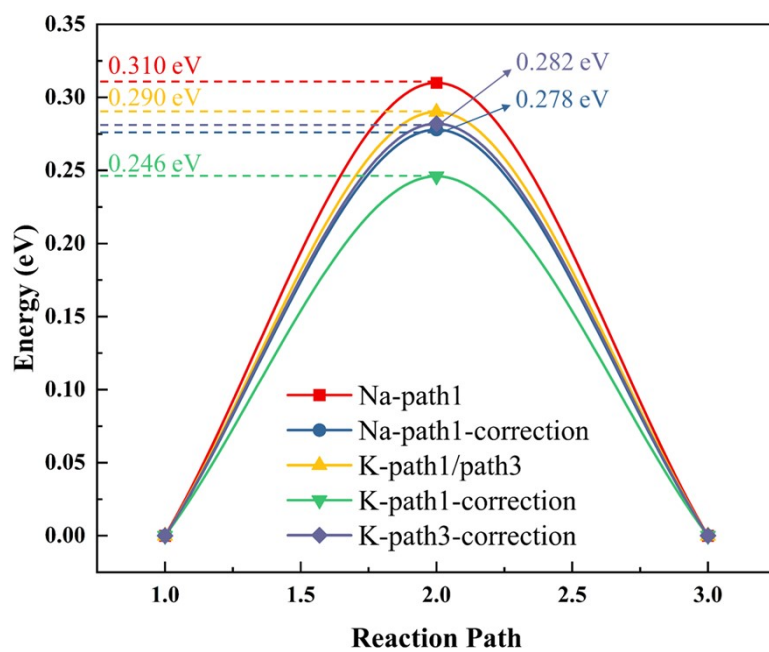


Fig. S15 Energy barriers and thermodynamically corrected energy barriers for the lowest energy barrier path of Na (path-1) and K (path-1 and path-3).

Considering the crucial role of entropy in calculation of ion migration barriers as it affects thermodynamic and kinetic properties of the migration process, free energy difference (ΔG) of ion migration processes is calculated according to the approach proposed by Nørskov *et al*¹. The equation is defined as:

$$\Delta G = \Delta E + \Delta E_{zpe} - T\Delta S + \Delta G_{pH} + \Delta G_U \#(1)$$

where ΔE is the adsorption energy, ΔE_{zpe} and ΔS are difference of zero-point energies and entropies between the adsorbed states, respectively. The value of pH significantly affects Gibbs free energy change for ion migration (ΔG_{pH}) on anode materials, which follows the equation “ $\Delta G_{pH} = k_B T \times \ln 10 \times pH$ ” (k_B is Boltzmann's constant, T is the temperature, and pH is the acidity of the solution). In our investigation, the value of pH is set to 0 to simulate an extreme acidic environment. As acidic conditions favor the performance of anode material, the ideal performance of the B_8N_2 monolayer could be observed under the condition of $pH = 0$. The potential (U) is also set to 0 volts in our study to simulate the behavior of the anode material in absence of an external voltage. During practical charging process of batteries, the external voltage could affect charging performance, where Gibbs free energy change (ΔG_U) is related to applied voltage (U) following the equation “ $\Delta G_U = -eU$ ” (e is charge), thus any external potential would reduce the ion migration barriers. The entropy change (ΔS) describes the degree of disorder in a system, which can be calculated from the partition function in statistical thermodynamics, including the contributions from five parameters of molecule (advection, rotation, vibration, electrons, and nucleus). However, commonly used software of first principles calculation, such as VASP^{2,3}, could not directly calculate entropy. We use Module 501 of the VASPKIT package⁴ to calculate entropies based on the frequency data output from VASP, and obtain the entropy change (ΔS).

References:

1. J. K. Nørskov, J. Rossmeisl, A. Logadottir, L. Lindqvist, J. R. Kitchin, T. Bligaard, and H. Jónsson, *J. Phys. Chem. B.*, 2004, **108**, 17886-17892.
2. G. Kresse and J. Hafner, *Phys. Rev. B*, 1993, **47**, 558–561.
3. G. Kresse and J. Furthmüller, *Phys. Rev. B*, 1996, **54**, 11169–11186.
4. V. Wang, N. Xu, J.-C. Liu, G. Tang and W.-T. Geng, *Comput. Phys. Commun.*, 2021, **267**, 108033.

Table. S1 Detailed values of bond length (in Å) and bond angle (in °) for optimized XH₄ (X=B₄, C, Si, Ge).

	X-H1	X-H2	X-H3	X-H4	H1-X-H2	H1-X-H3	H1-X-H4	H2-X-H3	H2-X-H4	H3-X-H4
B ₄ H ₄	1.186	1.187	1.187	1.188	109.483	109.483	109.483	109.46	109.469	109.453
[B ₄ H ₄] ⁻	1.206	1.206	1.206	1.206	117.772	105.519	105.455	105.519	117.772	105.519
[B ₄ H ₄] ⁺	1.192	1.178	1.192	1.179	104.208	107.045	104.029	104.029	104.208	131.551
CH ₄	1.093	1.093	1.093	1.093	109.471	109.471	109.471	109.471	109.471	109.471
[CH ₄] ⁻	1.16	1.16	1.16	1.16	109.471	109.471	109.471	109.471	109.471	109.471
[CH ₄] ⁺	1.125	1.125	1.124	1.124	96.71	96.67	96.694	96.751	96.751	104.077
SiH ₄	1.486	1.486	1.486	1.486	109.471	109.471	109.471	109.471	109.471	109.471
[SiH ₄] ⁻	1.637	1.636	1.53	1.529	93.089	93.087	92.986	92.984	103.488	170.184
[SiH ₄] ⁺	1.466	1.466	1.582	1.581	126.79	113.207	113.201	56.805	113.186	113.203
GeH ₄	1.538	1.538	1.538	1.538	109.471	109.471	109.471	109.471	109.471	109.471
[GeH ₄] ⁻	1.781	1.774	1.601	1.601	169.768	93.321	93.366	93.366	98.308	93.321
[GeH ₄] ⁺	1.519	1.519	1.66	1.66	127.842	112.505	59.182	112.478	112.381	112.558

Table S2 The adsorption energies for Li/Na/K ions on the B₈N₂ monolayer calculated with and without van der Waals (VDW) correction.

Adsorption Energies	Li	Na	K
With VDW	-0.44 eV	-0.52 eV	-1.21 eV
Without VDW	-0.42 eV	-0.47 eV	-0.98 eV